Perhalogenation and Percyanation of Coronene for Characterization of the New Efficient Organic Semiconductors for Charge Transport

Marius Ousmanou Bouba
University of Maroua
Fridolin Tchangnwa Nya (nyafridolin@yahoo.fr)
University of Maroua https://orcid.org/0000-0002-8882-6987
Alhadji Malloum
University of the Free State - Bloemfontein Campus: University of the Free State
Jeanet Conradie
University of the Free State - Bloemfontein Campus: University of the Free State
Jean Marie Ndjaka
University of Yaounde I: Universite de Yaounde I

Research Article

Keywords: Perhalogenated coronene , Percyanocoronene , Charge transport , n-type material , Organic semicondoctor

Posted Date: July 27th, 2021

DOI: https://doi.org/10.21203/rs.3.rs-730715/v1

Noname manuscript No.
(will be inserted by the editor)

Perhalogenation and percyanation of coronene for characterization of the new efficient organic semiconductors for charge transport.

Marius Ousmanou Bouba[1] · **Fridolin Tchangnwa Nya**[1] ⋆ · **Alhadji Malloum**[1,2] · **Jeanet Conradie**[2] · **Jean Marie Ndjaka**[3]

the date of receipt and acceptance should be inserted later

Abstract We have investigated the structures, electronic properties, hole and electron mobilities of perfluorinated, perchlorinated and percyanated coronene molecules, using the density functional theory (DFT) at the B3LYP-D3/6-311++G(d,p) and ωB97XD/6-311++G(d,p) levels and Markus-Hush charge transfer theory. The calculated geometric parameters for coronene and perchlorocoronene are in good agreement with the experimental data. Our theoretical investigations have shown B3LYP-D3 functional is suitable to well define vibrational assignments for studied molecules. We have shown that the per-halogenation and per-cyanation of coronene increases the adiabatic electron affinities (AEAs) and reduces the LUMO levels and the hole mobilities thus indicating an ambipolar behavior and air-stable material. We have shown that the percyanation of coronene is a promising pathway for the design of new materials useful in optoelectronics.

Keywords Perhalogenated coronene · Percyanocoronene · Charge transport · n-type material · Organic semicondoctor

1 Introduction

Nowadays, scientific research in the field of materials sciences is mainly focused on the characterization of the electronic and optical properties of organic semiconductors (OSCs). Their inorganic counterparts consisting of silicon or gallium arsenide, which for the most are polluting, very expensive and difficult to synthesize. Organic compounds have the benefit to be flexible, less expensive, easy to synthesize and have extraordinary optoelectronic properties. This allows the developement of organic field-effect transistors (OFETs), organic solar cells (OSCs) [1], polymers light emitting diode (PLEDs) and organic light emitting diodes (OLEDs) [2]. In the past few decades, great interest has been devoted to the study of p-type organic compounds (hole transporting). Promoting the industrial development of organic semiconductors (OSCs), and the p-chanel OFETs such as pentacene, tetracene, hexathiapentacene (HTP), ruberene and 5,11-dichlorotetracene(DCT) [3,4] with good air-stability and hole mobilities up to 1 $cm^2V^{-1}s^{-1}$ [5]. Unfortunally, compared to their p-channel counterparts, the development of n-type organic semiconductors has been lagged behind due to the instability of anion radicals in air and also because of the high injection barrier [5,6]. The method of solving this issue is to provide organic n-type semiconductors with a low LUMO level. [7]. The n-type OSCs play an important role in ambipolar transistors. Thus, the characterization of ambipolar compounds stable in air remains a constant and permanent challenge.
Several theoretical and experimental investigations have shown that, depending on their concentration, a good strategy for obtaining ambipolar n-channel OSCs is to functionalize p-type compounds with bromine, fluorine or cyanide groups [8,9]. Coronene is a typical case of an organic compound from the polycyclic aromatic hydrocarbons (PAHs) family [10]. It is a useful material in nonlinear optic (NLO), as conductor [11,12,13,14,15,16,17], in organic electronics as organic transistors [18], as photo detectors and as solar cells [19,20]. Theoretical investigations made by Sanyal *et al* [2] have shown that coronene is the typical p-type material (with hole mobility 15 times than the electron mobility). Further analysis showed that attachement of imide groups (especially the tetraimide) is the good strategy to obtain the ambipolar material from coronene. Sancho-García and Pérez-Jiménez [21] showed that perfluorination of coronene does not significally induces the ambipolar bihavior (hole mobility 15 times, than the electron mobility).

Beyond the state of the art, we explore the effects of per-functionalization of coronene with electron-withdrawing groups of chlorine (-Cl) and cyanide (-CN) (see Fig. 1) on their geometrical, electronic structures, stability and charge transport properties using theoretical methods. We expect that this investigation can provide good guidelines for designing novel n-channel organic semiconductors with high charge transport properties and air stability.

⋆ Corresponding author
E-mail: nyafridolin@yahoo.fr

1. University of Maroua, Faculty of Science, Department of Physics, P.O. Box 814 Maroua, Cameroon.Materials Science Laboratory.
2. Department of Chemistry, University of the Free State, PO Box 339, Bloemfontein, 9300, South Africa.
3. University of Yaoundé I, Faculty of Science, Department of Physics, P.O. Box 812 Yaounde, Cameroun.

2 Theoretical and computational models

2.1 Theoretical models

2.1.1 Electronic properties

The vertical electron affinity and ionization potential (VEA and VIP, respectively), adiabatic electron affinity and ionization potential (AEA and AIP, respectively), reorganization energy for electron λ_e and reorganization energy for hole λ_h are calculated from the electronic energies and described, respectively by the following equations [21,22,23,24,25] :

$$VEA = E_n(Q_n) - E_a(Q_n), \tag{1}$$

$$VIP = E_c(Q_n) - E_n(Q_n), \tag{2}$$

$$AEA = E_n(Q_n) - E_a(Q_a), \tag{3}$$

$$AIP = E_c(Q_c) - E_n(Q_n), \tag{4}$$

$$\lambda_e = \big[E_a(Q_n) - E_a(Q_a)\big] + \big[E_n(Q_a) - E_n(Q_n)\big], \tag{5}$$

and

$$\lambda_h = \big[E_c(Q_n) - E_c(Q_c)\big] + \big[E_n(Q_c) - E_n(Q_n)\big]. \tag{6}$$

Where :

- $E_n(Q_n)$ is the total energy of the neutral molecule, calculated from the optimized structure of the neutral molecule;
- $E_a(Q_a)$ and $E_c(Q_c)$ are the total energies of the molecule in the anion and cation states, calculated from the optimized structure of the geometry in the anion and cation state, respectively;
- $E_n(Q_a)$ and $E_n(Q_c)$ are the total energies of the neutral molecule, calculated from the optimized structure of the molecule in the anion and cation state, respectively;
- $E_a(Q_n)$ and $E_c(Q_n)$ are the total energies of the anion and cation, respectively, calculated from the optimized structure of the molecule taken in the neutral state.

2.1.2 Charge transport properties

There are several theoretical models to describe the transport properties in organic materials. The model used in this work to perform the charge transfer rate is the Marcus-Hush theory [26,27] and so called the hopping model. The Marcus-Hush approach was used for two main reasons. First, it describes the charge transfer through the intermolecular interactions between adjacent molecules of a crystal system by the hopping mecanism. Second, it correctly describes the anisotropic mobilities for organic molecular compounds [4].
The charge transfer rate K, according to the electronic hopping mechanism is given as follow [26,27]

$$K = \frac{V_{eff}^2}{\hbar}\sqrt{\frac{\pi}{\lambda K_B T}}exp\left(\frac{-\lambda}{4K_B T}\right). \tag{7}$$

V_{eff} is the effective intermolecular coupling energy between two adjacent dimers of the crystal, K_B is the Boltzmann constant, T is the temperature (in our case, it was set at 298.15 K).
The drift mobility of the charge carriers is calculated according to a random hopping model, known as the Einstein relation [28] and is given by

$$\mu_{drift} = \frac{eR^2K}{2K_BT}. \tag{8}$$

Where, e is the elementary charge and R, the distance between the considered monomers. The effective charge transfer integral V_{eff} is performed according to Eq. 9. It principally depends on transfer integral V_{12}, on overlap integral S_{12} between the fragments considered and on site energies ε_1 and ε_2 of the two molecular orbitals where charges are localized [2]:

$$V_{eff} = \frac{V_{12} - \frac{1}{2}(\varepsilon_1 + \varepsilon_2)S_{12}}{1 - S_{12}^2}. \tag{9}$$

With,

$$V_{12} = \langle \psi_1^{H/L} | \hat{H}_{ks} | \psi_2^{H/L} \rangle \tag{10}$$

$$S_{12} = \langle \psi_1^{H/L} | \psi_2^{H/L} \rangle, \tag{11}$$

$$\varepsilon_1 = \langle \psi_1^{H/L} | \hat{H}_{ks} | \psi_1^{H/L} \rangle, \tag{12}$$

$$\varepsilon_2 = \langle \psi_2^{H/L} | \hat{H}_{ks} | \psi_2^{H/L} \rangle. \tag{13}$$

In these equations, $\psi_1^{H/L}$ and $\psi_2^{H/L}$ represent the highest occupied molecular orbitals (HOMO) / lowest unoccupied molecular orbital (LUMO) of the two monomers considered and $\hat{H}_{ks}$ is the Kohn-Sham Hamiltonian of the dimer system used for the calculation of charge transfer.

2.2 Computational details

The geometry optimization and electronic properties of studied molecules was carried out using the dispersion-corrected functionals B3LYP-D3 [29,30] and the long-range dispersion corrected hybrid exchange and correlation functional ωB97XD [31] using the 6-311++G(d,p) basis set. The intermolecular coupling energies between the dimers have been calculated at the same levels. The choice of DFT is justified by the fact that:

- It offers an excellent compromise between computation time and electronic correlation [32];
- It is well known that the B3LYP hybrid fuctional offers the good description of geometric stucture in charge transfer mechanism [33,34,35,36]. And it is often used in the literature to easily predict the reorganization energies of aromatic π-conjugated organic molecules [37,38].

All calculations in this document are made using *Gaussian 16* software package [39]. The coupling energies, V_{eff} (see Eq. 9) were calculated with the aid of calc_J package [40] which uses the direct calculation method (see refs [41,42] for more details).

3 Structures, vibrations and electronic properties

3.1 Geometric and electronic structure

The geometries of experimental single coronene and perchlorocoronene molecules were extracted from their crystalline structure and presented as follow: a=16.119 Å, b=4.702 Å, c=10.102 Å, α=90°, β=110.9°, γ=90°, space group P21/a for coronene [10] and a=22.217 Å, b=8.214 Å c=12.921 Å, α=90°, β=90°, γ=90°, space group Cmca for perchlorocoronene [43]. The crystallographic information file (CIF) of these two crystalline structures were taken from Cambridge structural database (CSD) (N° 1129883 and N° 1181564, respectively). The molecules of perfluorocoronene and percyanocoronene have not been synthetised yet and were constructed intituively starting from the molecular geometry of coronene molecule.

Fig. 1 shows the optimized ground state structure of studied molecules. It is important to specify that the figures optimized at the B3LYP-D3 and ωB97XD levels are nearly identical and do not present any major differences with bond lengths differing more than 0.012, 0.011, 0.012 and 0.012 Å for coronene, perfluorocoronene, perchlorocoronene and percyanocoronene, respectively (see Tables S1-S4). As presented, the substitution of the hydrogen by chlorine atoms or cyano group induces a distrosion of the initial geometry, which is not the case for the substitution by fluorine atoms. According to Erkoç *et al.* [44], these effects can be attribuated to the size of the different atoms used. Tables S1-S4 also collect the neutral, anionic and cationic bond lengths of studied molecules, using the B3LYP-D3 and ωB97XD functionals. In order to well define the effect of B3LYP-D3 and ωB97XD functioanls on optimized bond lenghts of coronene and perchlorocoronene molecules, we calculated the average deviation ΔR throught the Eq 14 as:

$$\Delta R = \frac{1}{N}\sum_{i}^{N}|R_i - R_i^{exp}|. \tag{14}$$

R_i and R_i^{exp} represent the calculated and experimental ith bond lengths for considered studied molecule. The computed ΔR_{B3LYP} and $\Delta R_{\omega B97XD}$ are respectively 0.014 and 0.014 Å for coronene and for perchlorocoronene it is 0.025 and 0.024 Å. By comparision, the bond lengths are slightly different than the experimental values for the two functionals used, showing that B3LYP-D3 and ωB97XD well define the geometry of coronene and perchlorocoronene molecules. In addition for the coronene molecule, the deviation between the calculated bond lengths of ground state and the experimental data range from 0 to 0.038 Å for B3LYP-D3 and from 0 to 0.036 Å for ωB97XD. For the perchlorocoronene molecule we show that the deviation between the calculated bond lengths of ground state and the experimental data range from 0.006 to 0.043 Å for B3LYP-D3 and from 0.005 to 0.052 Å for ωB97XD. This shows that the functionals used are suitable for study the titled molecules.

The bond length variations between neutral and anionic/cationic geometries for studied molecules have been plotted with the values given in Tables S1-S4 and shown in Fig. 2. The oxidation/reduction curves correspond to the difference between the bond length of the neutral state and its corresponding in the cationic/anionic state. As presented, the variations in bond length appear on almost all of the entire molecules. This is certainly due to the presence of the extended π-system [45]. To quantitatively elaborate the geometric distortions during charge transfer, we have calculated the magnitude of bond length-change ($\sum|\Delta(N-A)|$ and $\sum|\Delta(N-C)|$) [7,45,46] during the reduction and oxidation processes respectively. The results show a $\sum|\Delta(N-A)|$ value of 0.348, 0.526, 0.496 and 0.311 Å at the B3LYP-D3/6-311++G(d,p) level and 0.415, 0.577, 0.566 and 0.425 Å at the ωB97XD/6-311++G(d,p) level. And a $\sum|\Delta(C-A)|$ value of 0.310, 0.472, 0.486 and 0.322 Å at the B3LYP-D3/6-311++G(d,p) level and 0.396, 0.565, 0.605 and 0.446 Å at the ωB97XD/6-311++G(d,p) level, for coronene, perfluorocoronene, perchlorocoronene and percyanocoronene respectively. The close values of the magnitude bond-length change during reduction and oxidation processes indicate a balanced charge transfer and the potentially close values of hole and electron reorganisation energies.

3.2 Vibrational analysis

Coronene, pefluorocoronene and perchlorocorone each contain 36 atoms, leading to 102 normal modes made up of 35 stretchings, 34 bendings and 33 torsions (out-of-plane). The percyanocoronene molecule has 48 atoms leading to 138 normal modes made up of 47 stretchings, 46 bendings and 45 torsions.

The computed IR spectra at the DFT/B3LYP-D3/6-311++G(d,p) and DFT/ωB97XD/6-311++G(d,p) levels are plotted and presented in Fig. 4. No imaginary frequency was observed; we can conclude that the molecular structures are stable and that a minimum position of the potential energy surface is obtained for each studied geometry [47]. A Comparison with calculated (unscaled) and experimental IR frequencies for coronene shows closer agreement at the B3LYP-D3 level than that obtained with ωB97XD (see Table 1). Thus, a more reliable assignment of IR modes of vibration can be carried out at the B3LYP-D3/6-311++G(d,p) level for coronene and related molecules.

The calculated frequencies, as well as the potential energy distributions (PEDs) as implemented in VEDA 4 program [48] of some specific vibrational modes for studied molecules are listed in Table 1 and discussed in this section. We noted a maximal absorption in the coronene molecule, strongly affected by a streching of the C-H bond (with PED contribution of 93%), centered at 3173.12 cm^{-1} and which coincides well with the experimental observation (3199.3 cm^{-1}). The perfunctionalization of the coronene with heteroatoms of fluorine, chlorine or with the cyano group induces a shift of the maximum peak towards frequencies respectively centered at 1390.6, 1321.25 and 1470.06 cm^{-1} and for which the vibrational assignments and PED contributions are collected in Table 1. We have also found the highest PED contributions for the respective cases of coronene, perfluorocoronene, and perchlorocoronene molecules of 93, 21 and −16 %, centered at 3173.1, 1678.3 and 719.10 and whose assignments are collected in the same table 1. Thus showing the effect of the perfunctionalization of the coronene molecule by the fluorine and chlorine heteroatoms on the intensity of the stretching effects of the peripheral C-X (X = F, Cl) bonds.

3.3 Frontier molecular orbitals (FMO).

In this section, we explain the charge carrier properties of studied molecules throught the spatial distribution of frontier molecular orbitbals [50]. The HOMO/LUMO orbitals as well as their corresponding energies were determined to study the efficiency of charge transfer, and also to study the major charge carriers. In order to compare our result with the experimental data, we have choosen to compute the HOMO-LUMO gap energies using three main DFT functionals, as B3LYP-D3, ωB97XD, HSE using the same basis set 6-311++G(d,p). We emphasis the performance of HSE functional in prediction of gap energy of molecular systems [51]. The calculated HOMO-LUMO gap of studied molecule are collected in Table 2 and discussed in this section. As seen, the gap energy of coronene shows a close agreement between B3LYP-D3, HSE methods, 4.00 and 3.63eV respectively and experimental data, 3.37 eV. While the ωB97XD functional overestimates the gap energies, it was shown that the B3LYP-D3 presents a good agreement with the experimental value. Thus, more realistic diagrams of molecular orbitals can be done at the DFT/B3LYP-D3/ 6-311++G(d,p) level.

As presented in Fig. 5, the spatial distribution of both molecular orbitals (HOMO and LUMO) are uniform in all the molecular geometry of studied compounds. Explaining that the charge carriers are uniformly distributed over the entire surface of the geometry. In addition, the studied compounds exhibit the π-type frontier molecular orbitals and mainly dominated by the p_z orbitals of the carbon atoms. From the same figure, it was noted that the gap energies and the LUMO level decrease during halogenation and cyanation. But it is not the case for the HOMO level. The calculated gap energies for coronene, perfluorinated and perchlorinated coronene are slightly higher than those performed by Sancho-García and Pérez-Jiménez [21] at the B_ALYP/def2-TZVP level (4.30, 4.10 and 3.54 eV, respectively). We emphasis in the fact that, the HOMO - LUMO gap energies were evaluated to study the nature of the compounds studied. It is well known that one of the crucial conditions for a semiconductor is that this latter must have an absorption range in the visible region (wavelength between 380 and 760 nm) [52]. In other words, the threshold wavelength of the photon which must ensure the electron to jump from HOMO to LUMO level is given by:

$$\lambda(nm) = \frac{1240}{E_{gap}(\text{eV})}, \tag{15}$$

where the numerator 1240 eV nm representes the product of Planck's constant(h, in eV s) by the celerity of light(c, in m/s) and E_{gap} is the HOMO - LUMO gap. Our B3LYP-D3 calculated absorption wavelength for coronene ($\lambda = 310nm$) agree well with those obtained experimentally ($\lambda = 377nm$) by the ultraviolet photoelectron spectroscopy (UPS) measurments [53]. Compared to coronene, we expected that percyanation of coronene causes a shift of this wavelength from the ultraviolet to visilble region. This is effectively the case for this compound for which λ is equal to 393 nm.

3.4 Electron affinity and ionization potential

We have reported in Table 2 the properties derived from the calculation of the electronic energies. Electron affinities, ionization potentials and intermolecular reorganization energies have been reported. Transport properties, holes and electrons injection capabilities of the organic semiconductor material can be explained by the ionization potentials (IPs) and electron affinities (EAs) [54,1]. As presented from this table, the close values of adiabatic and vertical energies at the two theoretical levels

show that geometric relaxations during charge injection are small [55]. Electron affinities increase after substitution of the different groups, which is not really suppressing with regard to the similar behavior for the energies of the LUMO level commented in the section 3.3. Our estimated vertical electron affinity/ionization potential of coronene are respectively 0.45/7.13 eV at the B3LYP-D3 and 0.24/7.26 eV at the ωB97XD levels, showing close agreement in comparison to the available experimental data (0.47/7.29 eV) from photoionisation threshold [53,56]. It is well known that, n-type organic semiconductors are characterized by high electron affinity [57,50]. In opposition to coronene, for which majority charge carriers are the holes [2], percyanocoronene are promising materials for charge transport by electrons (ambipolar materials). In addition, Chao *et al.* [58] signaled that for the air-stable electron carriers, the calculated adiabatic electron affinity (AEA) must be close to or larger than 2.8 eV. It can be seen that the obtained AEAs values for percyanocoronene at the two levels of theory B3LYP-D3 and ωB97XD are 4.66 and 4.52 eV, respectively. This indicates an air-stable material.

3.5 Partial conclusion

In this section, we have shown the important effect of perfluorination, perchlorination and percyanation of the coronene molecule on the geometric and electronic properties. We have emphasized the fact that the proposed percyanocoronene molecule has good electronic properties through its gap energy and that the latter is stable in air. The B3LYP-D3 functional used for the calculation of bond length and IR spectra offers an excellent agreement with the experiment, thus showing the performance of the B3LYP-D3/6-311++G(d,p) method and its reliability in our results.

4 Charge transport properties

4.1 Reorganization energies

As presented in Eqs. 5 and 6, and according to Marcus-Hush charge transfer theory, we have calculated and reported in Table 2, the reorganization energies of charge carrier for all studied molecules. We need to mention that the calculated reorganization energies of coronene and related molecules do not take into account the external reorganisation energy due to the polarization effect. The reason is that, the calculation of this energy is very dificult due to the presence of the other molecules of crystal in the solid state [59,60,61,62]. The reorganisation energies for all the studied molecules show that λ_e is higher than λ_h. Thus, the creation of holes is more favorable in these materials than the introduction of electrons, which leads to a mobility by the holes (μ_h). We emphasise in the case of coronene that our estimates of the electron and hole reorganisation energies at the B3LYP-D3/6-311++G(d,p) level (λ_e=170 meV, and λ_h=128 meV are slightly lower than previous estimates at the B3LYP/6-311++G(d,p) level (λ_e = 172 meV, λ_h= 129 meV) [2]. This difference represents the energy of the 3rd order Grimme correction (D3 term)[63] which was used in our results to obtain more refined energy values. However, in comparison with the functional B3LYP-D3, the estimated values of the reorganization energies at the ωB97XD/6-311++G(d,p) level are very high, thus showing an overestimation of these energies. We also noted that the reorganization energies of the holes are very close to those of the electrons regardless of the method used. This result, therefore, confirms that:

i the charge transport are balanced between the holes and the electrons (see section 3.1);
ii the geometric distortions during the electron transfer (from neutral state to anionic state) are identical to the geometric distortion during the hole transfer (from neutral state to cationic state).

4.2 Charge carriers mobility

4.2.1 Calculations in dimers systems

We summarized in Table 3, all properties related to the charge transport of the optimized dimers obtained by halogenation and cyanation of coronene (see Fig. 3). The coupling energies (V_{ij} and V_{eff}) were calculated using two different levels of theory in order to show a close dependence on the method used, and the important contribution of the energy of dispersion interactions in π-stacked dimers. We noted for the case of the coronene dimer that our results obtained at the B3LYP-D3/6-311++G(d, p) level of theory shows a close agreement with the theoretical previous estimates at the PBEPBE/TZ2P level [2]. Thus showing the performance of calc_J package in the prediction of charge transfer properties. The equilibrium interaction distances, R_{eq} (between the centroids of each monomer) were calculated and compared to those obtained from theoretical predictions. Our results obtained at the B3LYP-D3 and ωB97XD levels for the coronene dimer are respectively 3.733 and 3.684 Å thus showing a close agreement with the results obtained by Sancho-García and Pérez-Jiménez [21], R_{eq} = 3.74 Å (at the B_ΛLYP-D3/def2-TZVP level), but slightly higher than those obtained by Sanyal *et al.* [2], R_{eq} = 3.45 Å (at the ωB97XD/6-311++G(d,p) level). As can be seen in the same Table 3, the equilibrium interaction distances for perchlorocoronene and percyanoronene dimers show high parallel shifts, thus indicating low charge transfer rates in these dimeric systems. We find that the calculated V_{eff} of hole at the B3LYP-D3 level is significantly larger than that of electron one for all the dimeric system studied, indicating a transport by holes. We noticed a significant increase in the adiabatic

electron affinity (AEA), a decrease in the energy of the LUMO level (See Table 2), and a considerable decrease in the mobility of the holes, due to the full substitution of the hydrogen atoms by the fluorine, chlorine, and cyanide electron-donor groups: thus indicating ambipolar behavior. In addition, it is important to note that lowering the LUMO level also reduces the hole injection barrier and promotes the development of n-type materials. Thus it is obvious that the cyanation of coronene appears to be a very promising path for the development of organic semiconductors (OSC).

5 Conclusion

In summary, we have theoretically investigated structures, electronic parameters and charge transport properties of perhalogenated and percyanated coronene. The DTF method was coupled to Marcus-Hush hopping charge transport model to describe the hole and electron mobilities. The geometric analysis indicates that the bond lengths are in good agreement with experimental data for coronene and perchlorocoronene. The calculated results reveal that, the introduction of halogens or cyanide groups (-CN) significally reduces the bang gap energy of coronene, stabilizes the frontier molecular orbital and enhance the air-stable materials. The obtained high mobility of electrons for percyanated coronene indicates that percyanocoronene is the promoted ambipolar material. In the present theoretical protocol, it was question for us to study for the first time the important effect of the electron-donor substituents of cyanide groups on the charge transport properties of coronene. Our results will thus allow to promote pathway towards the new ambipolar materials derived from coronene and potentially useful in the field of optoelectronic.

Acknowledgements The authors are grateful to the Center for High Performance Computing (CHPC), South Africa, for granting them access to their clusters and computational resources.

Authors' contribution Marius Bouba Ousmanou: conceptualization; investigation; methodology; formal analysis; writing-original draft. Fridolin Tchangnwa Nya: conceptualization; investigation; methodology; writing-review and editing; supervision. Alhadji Malloum: writing-review and editing. Jeanet Conradie: writing-review and editing. Jean Marie Ndjaka: writing-review and editing.

Funding No funds or grants were received.

Data availability All data generated or analysed during this study are included in this published article (and it supplementary information file).

Declarations

Conflict of interest The authors declare that they have no conflict of interest.

Ethical approval This article does not contain any studies involving animals performed by any of the author.

Consent to participate All the co-authors consent to participate.

Consent to publish All the co-authors consent to publish.

References

1. S.R. Sahoo, S. Sharma, S. Sahu, Journal of Molecular Modeling **26**(1), 1 (2020). DOI 10.1007/s00894-019-4251-9
2. S. Sanyal, A.K. Manna, S.K. Pati, Journal of Physical Chemistry C **117**(2), 825 (2013). DOI 10.1021/jp310362c
3. H. Moon, R. Zeis, E.J. Borkent, C. Besnard, A.J. Lovinger, T. Siegrist, C. Kloc, Z. Bao, Journal of the American Chemical Society **126**(47), 15322 (2004). DOI 10.1021/ja045208p
4. S.H. Wen, A. Li, J. Song, W.Q. Deng, K.L. Han, W.A. Goddard, Journal of Physical Chemistry B **113**(26), 8813 (2009). DOI 10.1021/jp900512s
5. L.F. Ji, J.X. Fan, S.F. Zhang, A.M. Ren, Physical Chemistry Chemical Physics **19**(21), 13978 (2017). DOI 10.1039/c7cp01114h
6. L.L. Chua, J. Zaumseil, J.F. Chang, E.C. Ou, P.K. Ho, H. Sirringhaus, R.H. Friend, Nature **434**(7030), 194 (2005). DOI 10.1038/nature03376
7. J. Yin, K. Chaitanya, X.H. Ju, Journal of Materials Research **31**(3), 337 (2016). DOI 10.1557/jmr.2016.8
8. G.R. Hutchison, M.A. Ratner, T.J. Marks, Journal of the American Chemical Society **127**(7), 2339 (2005). DOI 10.1021/ja0461421
9. H. Geng, Y. Niu, Q. Peng, Z. Shuai, V. Coropceanu, J.L. Brédas, Journal of Chemical Physics **135**(10), 1 (2011). DOI 10.1063/1.3632105
10. J. Fawcett, J. Trotter, Proceedings of the Royal Society of London. Series A. Mathematical and Physical Sciences **289**(1418), 366 (2014). DOI 10.1098/rspa.1966.0017
11. G.W. Ejuh, N. Samuel, T.N. Fridolin, N.J. Marie, Materials Letters **178**, 221 (2016). DOI 10.1016/j.matlet.2016.04.097. URL http://dx.doi.org/10.1016/j.matlet.2016.04.097
12. I. Guezguez, A. Ayadi, K. Ordon, K. Iliopoulos, D.G. Branzea, A. Migalska-Zalas, M. Makowska-Janusik, A. El-Ghayoury, B. Sahraoui, Journal of Physical Chemistry C **118**(14), 7545 (2014). DOI 10.1021/jp412204f
13. L. Jensen, P.T. Van Duijnen, J.G. Snijders, D.P. Chong, Chemical Physics Letters **359**(5-6), 524 (2002). DOI 10.1016/S0009-2614(02)00739-X
14. S.S. Naghavi, T. Gruhn, V. Alijani, G.H. Fecher, C. Felser, K. Medjanik, D. Kutnyakhov, S.A. Nepijko, G. Schönhense, R. Rieger, M. Baumgarten, K. Müllen, Journal of Molecular Spectroscopy **265**(2), 95 (2011). DOI 10.1016/j.jms.2010.12.004

15. Rudiono, M. Takeuchi, Japanese Journal of Applied Physics, Part 2: Letters **36**(2 PART A), 127 (1997). DOI 10.1143/jjap.36.l127
16. N. Tyutyulkov, S. Karabunarliev, K. Müllen, M. Baumgarten, Synthetic Metals **53**(2), 205 (1993). DOI 10.1016/0379-6779(93)90891-Y
17. J. Friedrich, D. Haarer, Angewandte Chemie International Edition in English **23**(2), 113 (1984). DOI 10.1002/anie.198401131
18. S.P. Ekern, A.G. Marshall, J. Szczepanski, M. Vala, Journal of Physical Chemistry A **102**(20), 3498 (1998). DOI 10.1021/jp980488e
19. S.H. Choi, Journal of Physics D: Applied Physics **50**(10) (2017). DOI 10.1088/1361-6463/aa5244
20. M. Richter, T. Heumüller, G.J. Matt, W. Heiss, C.J. Brabec, Advanced Energy Materials **7**(10) (2017). DOI 10.1002/aenm.201601574
21. J.C. Sancho-García, A.J. Pérez-Jiménez, Journal of Chemical Physics **141**(13), 134708 (2014). DOI 10.1063/1.4897205
22. L. Wang, P. Li, B. Xu, H. Zhang, W. Tian, Organic Electronics **15**(10), 2476 (2014). DOI 10.1016/j.orgel.2014.07.003
23. F. de Proft, P. Geerlings, Chem. Rev. **101**(5), 1451 (2001)
24. C.G. Zhan, J.A. Nichols, D.A. Dixon, Journal of Physical Chemistry A **107**(20), 4184 (2003). DOI 10.1021/jp0225774
25. S. Arulmozhiraja, T. Fujii, H. Tokiwa, Journal of Physical Chemistry A **104**(30), 7068 (2000). DOI 10.1021/jp994237x
26. N.S. Hush, The Journal of Chemical Physics **28**(5), 962 (1958). DOI 10.1063/1.1744305
27. R.A. Marcus, Reviews of Modern Physics **65**, 599 (1993)
28. H. Gao, C. Qin, H. Zhang, S. Wu, Z.M. Su, Y. Wang, Journal of Physical Chemistry A **112**(38), 9097 (2008). DOI 10.1021/jp804308e
29. D. Feller, Journal of Computational Chemistry **17**(13), 1571 (1996)
30. K.L. Schuchardt, B.T. Didier, T. Elsethagen, L. Sun, V. Gurumoorthi, J. Chase, J. Li, T.L. Windus, Journal of Chemical Information and Modeling **47**(3), 1045 (2007). DOI 10.1021/ci600510j
31. M.H.G. J. Chai, Journal of Chemical Theory and Computation **9**(1), 263 (2008). DOI 10.1021/ct300715s
32. O. Holtomo, M. Nsangou, J.J. Fifen, O. Motapon, Journal of Molecular Graphics and Modelling **92**, 100 (2019). DOI 10.1016/j.jmgm.2019.06.016. URL https://doi.org/10.1016/j.jmgm.2019.06.016
33. X.K. Chen, L.Y. Zou, S. Huang, C.G. Min, A.M. Ren, J.K. Feng, C.C. Sun, Organic Electronics **12**(7), 1198 (2011). DOI 10.1016/j.orgel.2011.03.029. URL http://dx.doi.org/10.1016/j.orgel.2011.03.029
34. A. Datta, S. Mohakud, S.K. Pati, Journal of Materials Chemistry **17**(19), 1933 (2007). DOI 10.1039/b700625j
35. S. Mohakud, A.P. Alex, S.K. Pati, Journal of Physical Chemistry C **114**(48), 20436 (2010). DOI 10.1021/jp1047503
36. Y. Guo, W. Wang, R. Shao, S. Yin, Computational and Theoretical Chemistry **1057**, 67 (2015). DOI 10.1016/j.comptc.2015.01.019. URL http://dx.doi.org/10.1016/j.comptc.2015.01.019
37. M. Carmen Ruiz Delgado, E.G. Kim, D.A. Da Silva Filho, J.L. Bredas, Journal of the American Chemical Society **132**(10), 3375 (2010). DOI 10.1021/ja908173x
38. P. Song, M. Fengcai, Journal of Physical Chemistry A **114**(5), 2230 (2010). DOI 10.1021/jp909594e
39. M. Frisch, G. Trucks, H. Schlegel, G. Scuseria, M. Robb, J. Cheeseman, G. Scalmani, V. Barone, G. Petersson, H. Nakatsuji, et al. Gaussian 16 (2016)
40. Brown, j. s. (2018). catnip (version 1.9). [software]. available from https://github.com/joshuasbrown/qc_tools.
41. E.F. Valeev, V. Coropceanu, D.A. Da Silva Filho, S. Salman, J.L. Brédas, Journal of the American Chemical Society **128**(30), 9882 (2006). DOI 10.1021/ja061827h
42. B. Baumeier, J. Kirkpatrick, D. Andrienko, Physical Chemistry Chemical Physics **12**(36), 11103 (2010). DOI 10.1039/c002337j
43. T. Baird, J.H. Gall, D.D. MacNicol, P.R. Mallinson, C.R. Michie, Journal of the Chemical Society, Chemical Communications (22), 1471 (1988). DOI 10.1039/C39880001471
44. S. Erkoç, F. Erkoç, L. Türker, Journal of Molecular Structure **538**(1-3), 91 (2000). DOI https://doi.org/10.1016/S0166-1280(00)00651-5
45. C. Zhao, Y. Guo, L. Guan, H. Ge, S. Yin, W. Wang, Synthetic Metals **188**, 146 (2014). DOI 10.1016/j.synthmet.2013.12.009
46. J. Yin, K. Chaitanya, X.H. Ju, Journal of Materials Chemistry C **3**(14), 3472 (2015). DOI 10.1039/c4tc02655a
47. L. Chen, C. Xu, X.F. Zhang, Journal of Molecular Structure: THEOCHEM **863**(1-3), 55 (2008). DOI 10.1016/j.theochem.2008.05.020
48. M.H. Jamróz, Spectrochimica Acta - Part A: Molecular and Biomolecular Spectroscopy **114**, 220 (2013). DOI 10.1016/j.saa.2013.05.096
49. M. Koshino, H. Kurata, S. Isoda, Ultramicroscopy **110**(12), 1465 (2010). DOI 10.1016/j.ultramic.2010.09.003. URL http://dx.doi.org/10.1016/j.ultramic.2010.09.003
50. S.F. Zhang, X.K. Chen, J.X. Fan, A.M. Ren, Organic Electronics **14**(2), 607 (2013). DOI 10.1016/j.orgel.2012.12.001
51. J. Heyd, G.E. Scuseria, M. Ernzerhof, Journal of Chemical Physics **118**(18), 8207 (2003). DOI 10.1063/1.1564060
52. L. Wang, W. Huang, R. Li, D. Gehrig, P.W. Blom, K. Landfester, K.A. Zhang, Angewandte Chemie - International Edition **55**(33), 9783 (2016). DOI 10.1002/anie.201603789
53. P.G. Schroeder, C.B. France, B.A. Parkinson, R. Schlaf, Journal of Applied Physics **91**(11), 9095 (2002). DOI 10.1063/1.1473217
54. G. Saranya, K. Navamani, K. Senthilkumar, Chemical Physics **433**, 48 (2014). DOI 10.1016/j.chemphys.2014.01.020
55. S.P. Adiga, D. Shukla, Journal of Physical Chemistry **114**, 2751 (2010)
56. M.A. Duncan, A.M. Knight, Y. Negishi, S. Nagao, Y. Nakamura, A. Kato, A. Nakajima, K. Kaya, Chemical Physics Letters **309**(1-2), 49 (1999). DOI 10.1016/S0009-2614(99)00662-4
57. Y. Shi, Y. Shi, H. Wei, H. Zhai, Y. Liu, New Journal of Chemistry **41**(18), 10251 (2017). DOI 10.1039/c7nj02590d
58. Y.C. Chang, M.Y. Kuo, C.P. Chen, H.F. Lu, I. Chao, Journal of Physical Chemistry C **114**(26), 11595 (2010). DOI 10.1021/jp1025625
59. J.E. Norton, J.L. Brédas, Journal of the American Chemical Society **130**(37), 12377 (2008). DOI 10.1021/ja8017797
60. D.P. McMahon, A. Troisi, Journal of Physical Chemistry Letters **1**(6), 941 (2010). DOI 10.1021/jz1001049
61. S. Di Motta, E. Di Donato, F. Negri, G. Orlandi, D. Fazzi, C. Castiglioni, Journal of the American Chemical Society **131**(18), 6591 (2009). DOI 10.1021/ja901101c
62. Y.F. Chang, Z.Y. Lu, L.J. An, J.P. Zhang, Journal of Physical Chemistry C **116**(1), 1195 (2012). DOI 10.1021/jp208063h
63. S. Grimme, J. Antony, S. Ehrlich, H. Krieg, Journal of Chemical Physics **132**(15) (2010). DOI 10.1063/1.3382344
64. D.M. Hudgins, S.A. Sandford, **5639**(98), 344 (2000)

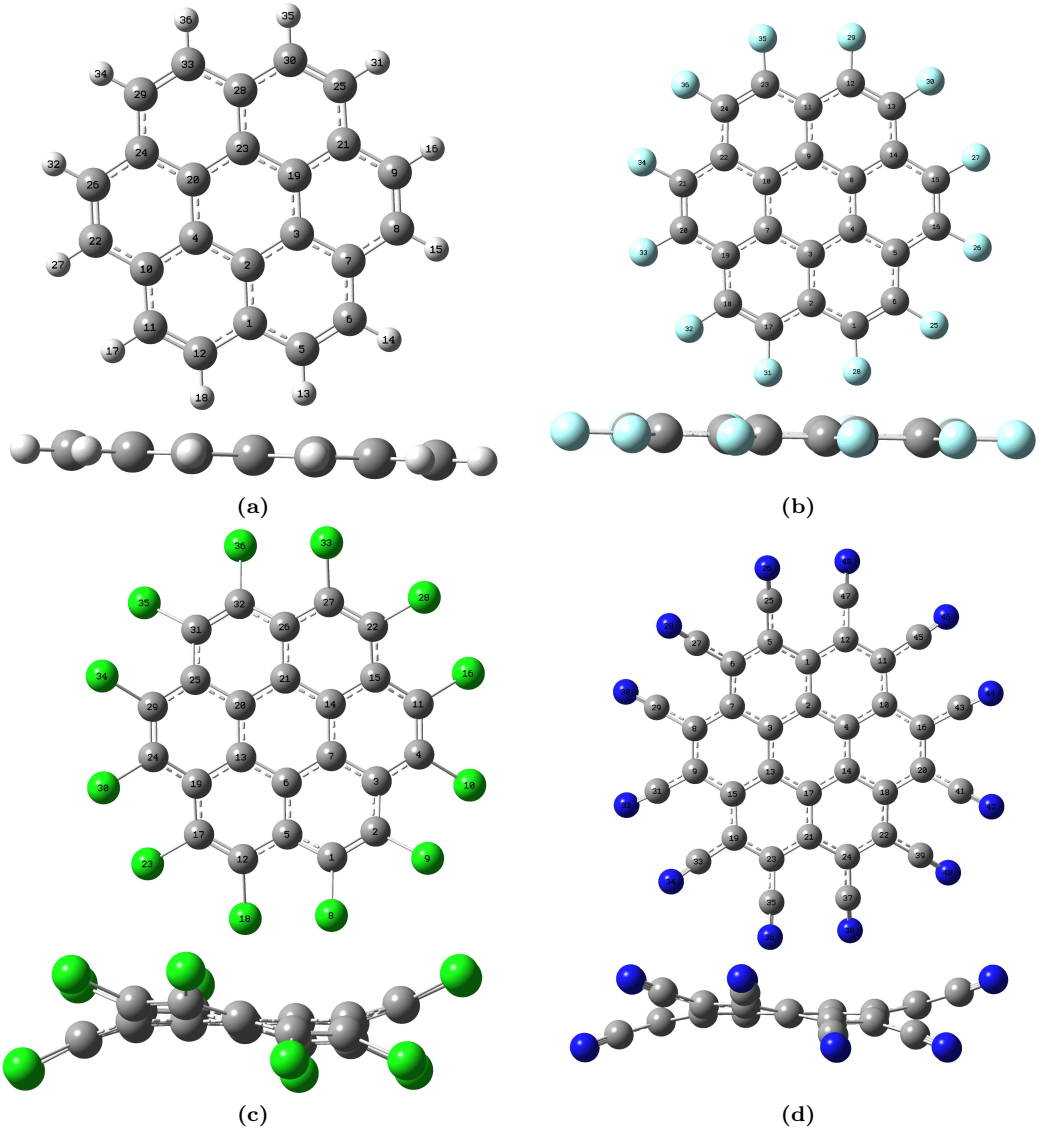

Fig. 1: Two views of monomeric structures of (a) coronene, (b) perfluorocoronene, (c) perchlorocoronene and (d) percyanocoronene, as optimized at the B3LYP-D3/6-311++G(d,p) level of theory. The ωB97XD/6-311++G(d,p) optimized geometries are similar within 0.012, 0.011, 0.012 and 0.109 Å for coronene, perfluorocoronene, perchlorocoronene and percyanocoronene, respectively and given in Fig. S1 .

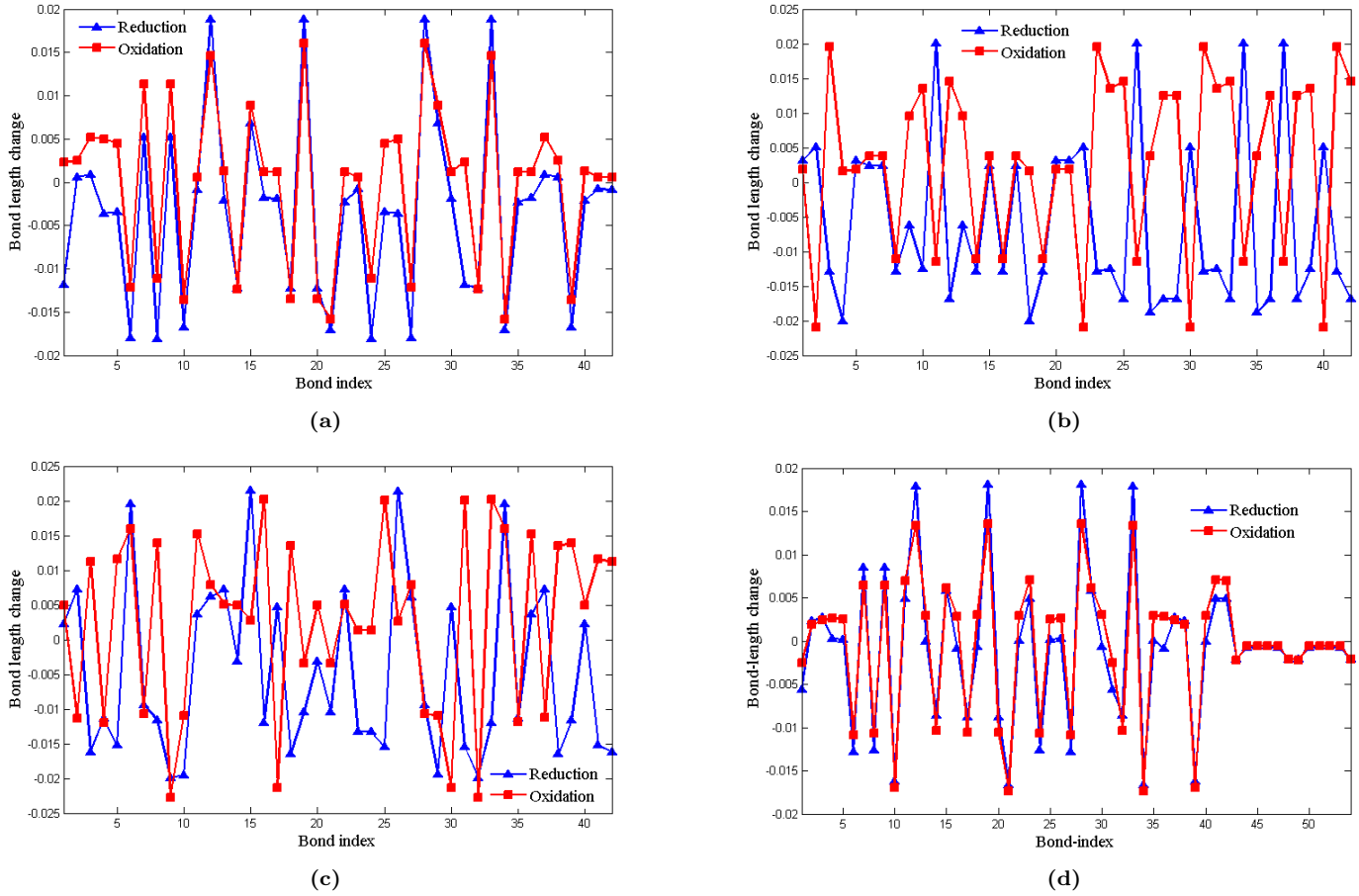

Fig. 2: B3LYP-D3/6-311++G(d,p)- calculated bond-length change (in Å) upon reduction and oxidation in of (a) coronene, (b) perfluorocoronene, (c) perchlorocoronene and (d) percyanocoronene. See Tables S1-S4 for calculated bond lengths.

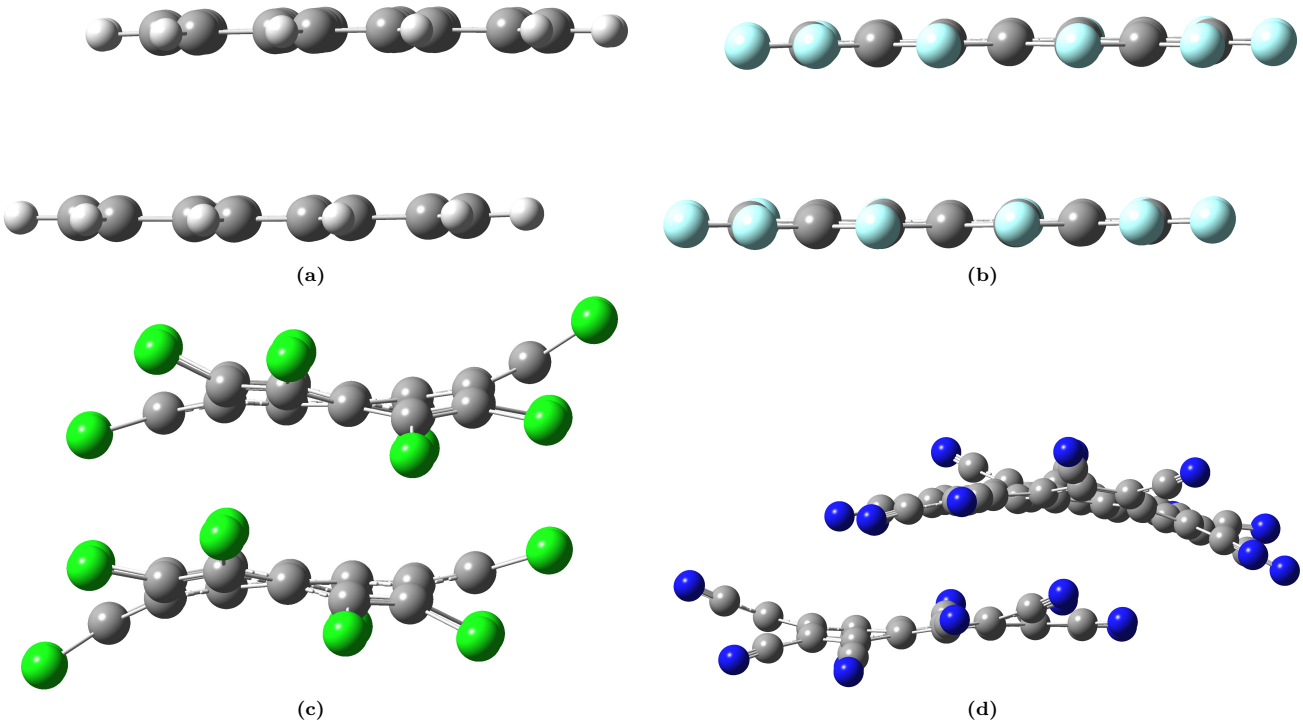

Fig. 3: Optimized dimeric structures of (a) coronene, (b) perfluorocoronene, (c) perchlorocoronene and (d) percyanocoronene, as optimized at the B3LYP-D3/6-311++G(d,p) level of theory.

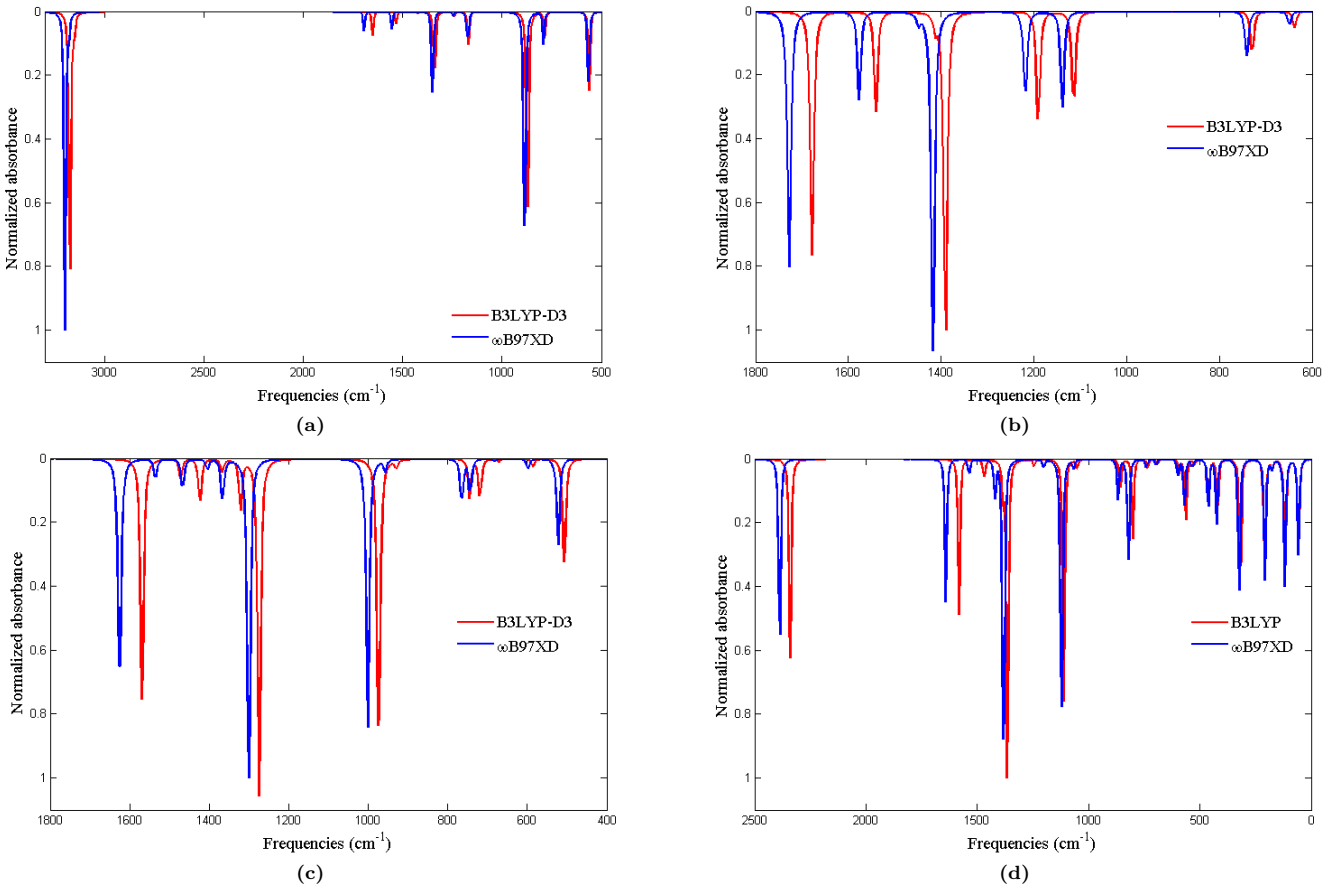

Fig. 4: Vibrational IR spectra of (a) coronene, (b) perfluorocoronene (c) perchlorocoronene and (d) percyanocoronene at the B3LYP-D3/6-311++G(d,p) and ωB97XD/6-311++G(d,p) levels.

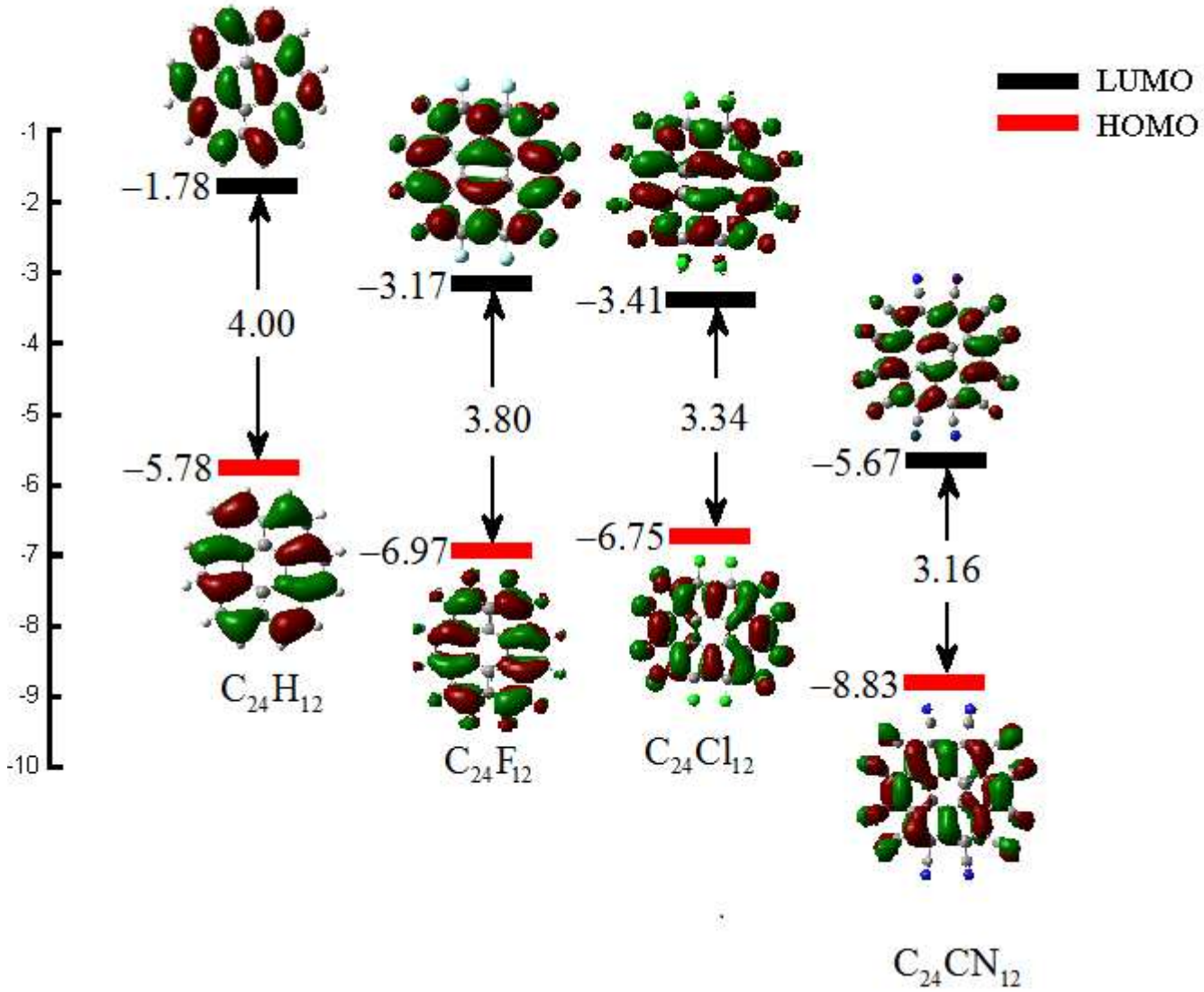

Fig. 5: Representation at the B3LYP-D3/6-311++G(d,p) level of frontier molecular orbitals (MOs) surfaces and their corresponding energies levels (in eV) for coronene, perfluorocoronene, perchlorocoronene and percyanocoronene molecules. The MOs at the ωB97XD/6-311++G(d,p) level of theory are presented in Fig. S3.

Table 1: Detailed assignments selected of theoretical frequencies for coronene, perfluorocoronene, perchlorocoronene and percyanocoronene along with potential energy distribution (PED $\geq$ 10%) at the B3LYP-D3/6-311++G(d,p) and ωB97XD/6-311++G(d,p) levels. δ: stretching, β: bending, and τ: torsion

	Frequencies (cm^{-1})			Vibrational assignment[a]
	B3LYP-D3	ωB97XD	Experiment[b]	
Coronene[c]				
	561.1	564.8	549.5	22τ(CCCC)
	785.3	790.6	772.3	22 β(CCC)
	871.4	857.7	885.7	-67τ(HCCC)
	1169.2	1137.4	1172.8	33β(HCCC)
	1340	1318.1	1349.9	-12β(HCC)
	1651.4	1607.7	1554.6	46 δ(CC)
	1652.3	1623.8	1693.2	-31 δ(CC); 13β(CCC)
	3173.1	3067.5	3199.3	93 δ(CH)
Perfluorocoronene				
	730	741		-10τ(CCCC)
	1114.1	1138.5		16β(CCC)
	1190.7	1218.6		-13β(CCC)
	1390.6	1418		-12δ(CC);13β(CCC)
	1540.4	1578.3		11β(CCC)
	1678.3	1728.7		-10δ(CC);21β(CCC);20β(CCC)
Perchlorocoronene				
	506.9	522.5		-15τ(ClCCC)
	719.1	743.2		-10β(CCCC); -16τ(ClCCC)
	745.2	764.9		11τ(ClCCC)
	973.9	1001.3		11δ(CC)
	1274.2	1300.3		-13δ(CC); -11δ(CC)
	1321.3	1361.7		11δ(CC)
	1423.3	1467.3		-12δ(CC)
	1568.9	1625.7		-10δ(CC)
Percyanocoronene				
	52.7	54.2		-22τ(CCCC)
	116.1	118		-36β(CCC)
	209.6	208.2		-27τ(CCCC)
	319	324.5		11τ(CCCN); 10τ(CCCC)
	419.9	424.4		11β(CCC); 14τ(CCCN)
	462.5	432		13τ(CCCC)
	563.1	569.7		15τ(CCCN); -26τ(CCCC)
	802.6	821.8		45τ(CCCC)
	858.5	867.3		-55δ(CC)
	1112.2	1122.5		12δ(CC); 24δ(CC)
	1364.3	1381.5		12δ(CC)
	1470.1	1422.7		29δ(CC); -22δ(CC)
	1582.8	1641.4		29δ(CC)
	2340.3	2388.2		-70δ(NC)

[a] This work at the B3LYP-D3/6-311++G(d,p) level of theory.
[b] Only available for coronene molecule (see ref [64])
[c] Unscaled values

Table 2: Estimates at B3LYP-D3/6-311++G(d,p) and ωB97XD/6-311++G(d,p) levels of reorganisation energies (λ_e) and (λ_h) for electrons and holes, respectively (in meV), adiabatic (A), vertical (V) ionization potential (IP, in eV), electron affinity (EA, in eV), HOMO - LUMO gap (E_{gap}, in eV) and the threshold wavelength of the HOMO - LUMO transition (λ, in nm) for studied molecules

	B3LYP-D3									ωB97XD									HSE
	VIP	AIP	VEA	AEA	E_{gap}	λ	λ_e	λ_h	λ_h/λ_e	VIP	AIP	VEA	AEA	E_{gap}	λ	λ_e	λ_h	λ_h/λ_e	E_{gap}
Coronene	7.13	7.07	0.45	0.54	4.00	310	170	128	0.76	7.36	7.26	0.24	0.36	7.31	170	247	200	0.81	3.63
Perfluorocoronene	8.31	8.18	1.83	1.97	3.80	327	286	273	0.95	8.52	8.34	1.59	1.77	7.08	175	357	367	1.03	3.42
Perchlorocoronene	7.87	7.76	2.30	2.43	3.34	372	265	211	0.80	8.22	8.06	2.11	2.29	6.62	187	338	325	0.96	2.95
Percyanocoronene	9.91	9.84	4.58	4.66	3.16	393	154	124	0.80	10.31	10.21	4.40	4.52	6.39	194	246	216	0.87	2.79

Table 3: Estimates of hole (h) and electron (e) effective electronic couplings (V_{eff}, in meV), the center-of-mass distance (R in Å) and the drift electrons/hole mobilities ($\mu_{e/h}$, in $cm^2V^{-1}s^{-1}$) for studied molecules.

	B3LYP-D3							ωB97XD						
	V(h)	V(e)	$V_{eff}(h)$	$V_{eff}(e)$	R	μ_h	μ_e	V(h)	V(e)	$V_{eff}(h)$	$V_{eff}(e)$	R	μ_h	μ_e
Coronene	379	57	186	41	3.733	12.6	0.36	517	89	245	88	3.684	8.50	0.63
Sanyal *et al* [a]	328	92	167	65	3.450	-	-							
Perfluorocoronene	337	-66	157	-37	3.574	1.38	0.07	462	-90	208	-66	3.542	0.83	0.09
Perchlorocoronene	45	-83	17	-53	4.242	0.05	0.24	58	-67	20	53	4.008	0.02	0.09
Percyanocoronene	208	-98	91	-52	5.659	7.36	1.59	117	-77	50	-49	5.358	0.61	0.41

[a] Results obtained for coronene at the PBE/TZ2P level of theory [2]

Supplementary Files

This is a list of supplementary files associated with this preprint. Click to download.

- Supporting.pdf